

# Journal of Biomedical Optics

BiomedicalOptics.SPIEDigitalLibrary.org

## Laser-induced breakdown spectroscopy as a potential tool for autocarbonization detection in laserosteotomy

Hamed Abbasi  
Georg Rauter  
Raphael Guzman  
Philippe C. Cattin  
Azhar Zam

# Laser-induced breakdown spectroscopy as a potential tool for autocarbonization detection in laserosteotomy

Hamed Abbasi,<sup>a,\*</sup> Georg Rauter,<sup>b</sup> Raphael Guzman,<sup>c</sup> Philippe C. Cattin,<sup>d</sup> and Azhar Zam<sup>a,\*</sup>

<sup>a</sup>Biomedical Laser and Optics Group, Department of Biomedical Engineering, University of Basel, Allschwil, Switzerland

<sup>b</sup>Bio-Inspired Robots for Medicine-Laboratory, Department of Biomedical Engineering, University of Basel, Allschwil, Switzerland

<sup>c</sup>Department of Neurosurgery, University Hospital Basel, Basel, Switzerland

<sup>d</sup>Center for Medical Image Analysis and Navigation, Department of Biomedical Engineering, University of Basel, Allschwil, Switzerland

**Abstract.** In laserosteotomy, it is vital to avoid thermal damage of the surrounding tissue, such as carbonization, since carbonization does not only deteriorate the ablation efficiency but also prolongs the healing process. The state-of-the-art method to avoid carbonization is irrigation systems; however, it is difficult to determine the desired flow rate of the air and cooling water based on previous experiments without online monitoring of the bone surface. Lack of such feedback during the ablation process can cause carbonization in case of a possible error in the irrigation system or slow down the cutting process when irrigating with too much cooling water. The aim of this paper is to examine laser-induced breakdown spectroscopy as a potential tool for autocarbonization detection in laserosteotomy. By monitoring the laser-driven plasma generated during nanosecond pulse ablation of porcine bone samples, carbonization is hypothesized to be detectable. For this, the collected spectra were analyzed based on variation of a specific pair of emission line ratios in both groups of samples: normal and carbonized bone. The results confirmed a high accuracy of over 95% in classifying normal and carbonized bone.

© 2018 Society of Photo-Optical Instrumentation Engineers (SPIE) [DOI: [10.1117/1.JBO.23.7.071206](https://doi.org/10.1117/1.JBO.23.7.071206)]

Keywords: laser-induced breakdown spectroscopy; laserosteotome; carbonized bone; smart surgery; feedback; differentiation.

Paper 170634SSR received Sep. 29, 2017; accepted for publication Feb. 12, 2018; published online Mar. 2, 2018.

## 1 Introduction

Over the past several years, there has been a particular interest in the development of laser surgery systems due to the advantages offered by laser-based cutting, including minimal invasiveness, noncontact interaction, precise and small cuts, functional cut geometry as well as less trauma.<sup>1–6</sup> Moreover, in comparison to other mechanical procedures, such as conventional surgery, bone showed faster healing after interventions with laserosteotomes.<sup>7</sup> Studying the effect of different laser parameters on quality and efficiency of laser cutting in both soft and hard tissues is a topic of present interest.<sup>8–13</sup> Although laserosteotomy has become a generally accepted technique in various surgical applications, this technique has two main drawbacks: lack of real-time information about depth of the cut and lack of information about the properties of the ablated tissue; as a result, critical structures of the body under or near the focal spot of the laser beam are prone to iatrogenic damage. In addition, to be a practical tool, clinical lasers have to be safe and effective in removing tissue with limited collateral damage. To reduce the thermal damage to the surrounding tissue, it is vital to use a cooling system to avoid carbonization. Carbonization happens when the tissue is heated up and all the water content is evaporated. Carbonization occurs not only in hard tissues but also in soft tissues. Carbonization not only reduces the ablation efficiency but also prolongs healing.<sup>14,15</sup>

Lack of real-time information about depth of the cut can be solved by combining the laser surgery system with a coaxial real-time optical coherence tomography setup,<sup>16,17</sup> and lack of information about the properties of the ablated tissue can be improved by connecting the system to an optical detection setup.<sup>18</sup> Therefore, having a real-time feedback method to detect the possible carbonization in case of any possible error in the irrigation system is needed.

The potential optical detection methods to investigate the properties of the tissues include optoacoustic-based measurements<sup>19,20</sup> and also spectroscopy-based measurements, including diffuse reflectance,<sup>21,22</sup> laser-induced breakdown,<sup>23–25</sup> Raman,<sup>26,27</sup> and fluorescence spectroscopy.<sup>28,29</sup> Among the above-mentioned optical methods, laser-induced breakdown spectroscopy (LIBS) showed its potential to detect the type of tissue with high accuracy. In LIBS, the light emitted from the ablation spot, which corresponds to the recombination spectra of ionized atoms and molecules, is collected with a spectrometer to resolve the atomic composition of the ablated sample. LIBS has been applied to differentiate between different tissue pairs with a high sensitivity and specificity (normally ranging from 70% to 100%), such as cartilage and cortical bone,<sup>30</sup> nerve and gland,<sup>31</sup> nerve and fat<sup>32</sup> as well as differentiation between oral soft and hard tissues.<sup>33</sup> Due to the compelling performance of LIBS in tissue characterization, we assume that applying LIBS also for detecting carbonization in laser surgery will be possible while tissue characterization can be performed in parallel.

\*Address all correspondence to: Hamed Abbasi, E-mail: [hamed.abbasi@unibas.ch](mailto:hamed.abbasi@unibas.ch); Azhar Zam, E-mail: [azhar.zam@unibas.ch](mailto:azhar.zam@unibas.ch)

The aim of this study is to differentiate between normal and carbonized hard porcine bone samples by monitoring the laser-driven plasma generated during a nanosecond pulse ablation using a frequency-doubled nanosecond Nd:YAG laser. A high-resolving power echelle spectrometer connected to an intensified CCD (ICCD) was employed to detect carbonization. The ICCD was capable of collecting LIBS signals with high temporal resolution (ps) and also short integration time (ns) to measure spectra for the classification of the samples. The analytical approach of calculating ratios of values of specific pairs of emission lines was taken to perform the differentiation between two groups of samples: normal (noncarbonized) and carbonized porcine bone. Then the sensitivity, specificity, and accuracy of the method were calculated afterward. Based on the results of the current study, we aim at proceeding LIBS-based carbonization detection also in real time. A successful real-time autodetection of carbonization in laserosteotomy will increase the safety of laserosteotomies. Additionally, this proof of principle study is intended to pave the way for *in vivo* experiments with an LIBS-based autocarbonization detection system in laser surgery.

## 2 Materials and Methods

### 2.1 Sample Preparation

Fresh porcine femur bone was used as a sample in this experiment. The bone samples were kept in a freezer between the slaughtering of the pig to the starting day of the experiment. The temperature of the freezer was set to  $-18^{\circ}\text{C}$ . Four hours before starting the experiment, the bones were moved from the freezer to the refrigerator ( $+4^{\circ}\text{C}$ ). Soft tissues were removed from the bone's surface using a surgical scalpel. Five bisected bones with the height of ca. 3 cm were used as samples. One half of each sample was irradiated by a microsecond Er:YAG laser (DPM-15, 3mikron, Pantec, Liechtenstein) with a pulse energy of 90 mJ and a 10-Hz repetition rate for 30 s without any cooling water to create a carbonized layer on the bone's surface; the other half of the bone remained untouched as a noncarbonized reference sample. To confirm bone carbonization and assess the carbon bonding, Raman spectroscopy was employed. Er:YAG bone ablation at  $3\ \mu\text{m}$  is based on absorption of the laser beam mainly by the water content of the bone. In contrast, with Nd:YAG ( $0.5\ \mu\text{m}$ ) lasers, ablation is mainly based on hydroxyapatite absorption.<sup>15,34</sup> Therefore, in Er:YAG ablation without rewetting the ablation area, the surface of the bone will carbonize faster.

### 2.2 Ethics Committee Approval

Ethics committee approval was not necessary for this work as the bone samples were commercially available as regular food obtained from the local slaughterhouse.

### 2.3 Laser Setup

Usually, LIBS measurement systems consist of two main parts: an ablating laser with an appropriate focusing setup and a spectrometer with the appropriate optics for collecting the emission light. A delay generator can be added to the setup optionally to have a time-resolved measurement with higher signal-to-noise ratio. Spatially resolved measurement is an alternative method to increase the signal-to-noise ratio in LIBS.<sup>35</sup> In this experiment, a flash-lamp-pumped Nd:YAG laser (Q-smart 450,

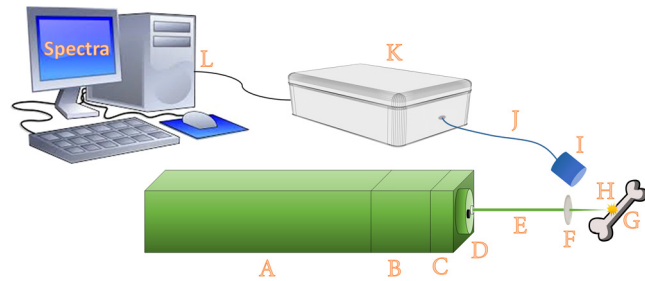


**Fig. 1** Schematics of the LIBS setup: A, laser (flash-lamp-pumped Nd:YAG), B, second-harmonic generator; C, harmonic separator; D, beam blocker; E, laser beam; F, focusing lens; G, bone sample; H, generated plasma; I, light collector; J, fiber optic; K, spectrometer (echelle); and L, computer.

Quantel, France) running in its second harmonics of 532 nm with 5-ns pulse duration was used to ablate both normal and carbonized bone samples. The 1064-nm mode of the beam was separated and blocked using a nonlinear crystal, and a beam blocker installed right after the harmonic generator, respectively. The laser was operated at 108 mJ per pulse and 1-Hz repetition rate. The initial output beam of the laser with 6.5-mm diameter was directly focused onto the sample's surface using an uncoated CaF<sub>2</sub> planoconvex lens (LA5458, Thorlabs) with a focal length of 80 mm.

### 2.4 Spectroscopy Setup

An echelle spectrometer with a wavelength range of 200 to 975 nm connected to an ICCD was used to reveal the spectral distribution of the laser-generated plasma light. The spectral resolution ( $\lambda/\Delta\lambda$ ) of the spectrometer was more than 4000. The CCD was cooled down to  $-30^{\circ}\text{C}$  to reduce the background noise level. A fiber optic with a  $50\text{-}\mu\text{m}$  core connected to a UV-NIR light collector with an  $F$ -number of 2 was used to guide the plasma light into the spectrometer. A gate delay of  $1\ \mu\text{s}$  between the laser shot and opening of the intensifier was applied to remove the continuum emission of the plasma. The gate width was set to  $200\ \mu\text{s}$ . Both gate delay and width were applied using the internal delay generator of the ICCD. Figure 1 shows the schematic of the LIBS setup.

### 2.5 Data Analysis

The bone samples were separated into two groups based on their carbonization: normal bone as a control group and carbonized bone as a test group. Each group consisted of five bones. One hundred shots were recorded from each side, 50 from the normal side and 50 from the carbonized side. In total, 500 spectra were recorded, 250 from each group. Then, to determine the elemental composition of the bone samples, the atomic emissions in the recorded LIBS spectra of both normal and carbonized bones were mapped with the National Institute of Standards and Technology atomic emission database.<sup>36</sup> After finding the related peaks of the different atomic elements, the wavelengths and the intensities of those reproducible peaks, which appeared in both groups, were stored in a separate file. Among the stored peaks, two peaks with the highest reproducible ratio difference in two groups of samples among all 500-recorded spectra were selected. Finally, the ratio between the intensity of the selected peak pairs was calculated, and a ratio threshold was found to have a maximum accuracy (maximum number of true positive

and also true negative). The analysis aims to determine the class membership within the normal and carbonized bone groups. This ratio analysis allows for more robust results, as it is more stable than the absolute or normalized intensity of emission lines in the spectra of a given tissue type.<sup>32</sup> The performance of the classifier was evaluated using receiver operating characteristic (ROC). Moreover, statistical parameters of the classifier, including true positive rate (sensitivity), true negative rate (specificity), positive predictive value (precision), negative predictive value, and accuracy, were calculated for each sample separately and also totally for all collected spectra.

### 3 Results

The elements detected in the bone samples through LIBS were identified as carbon (C), hydrogen (H), oxygen (O), calcium (Ca), sodium (Na), magnesium (Mg), zinc (Zn), and strontium (Sr). In addition to the atomic emission line of carbon, a molecular line of carbon-to-carbon bonding ( $C_2$ ) was also observed. This result is in line with results described in literature.<sup>30–32,37–44</sup> Note that the collected spectra may include emission lines of the elements found in the ambient air. Interestingly, the higher concentration of carbon in carbonized samples was not only observed in the average intensity of pure carbon emission line (13.77 for carbonized samples as compared with 3.15 for normal samples) but also in the carbon-related molecular emissions of the  $C_2$  (10.12 for carbonized samples as compared with 4.38 for normal samples). Moreover, a reduction in the emission intensity of the hydrogen line was observed in the carbonized sample compared to the normal one (from 9.08 to 5.05). Decreasing hydrogen emission intensity and increasing carbon emission intensity seem to indicate that the bone has dried out and will be followed by subsequent carbonization if not properly rehydrated before continuing with the laser ablation. In addition to the atomic and molecular LIBS, Raman spectroscopy results also show a change in the carbon bonding. The

Raman spectra of normal and carbonized bones are shown in Fig. 2.

As shown in Fig. 2, the Raman spectra of normal and carbonized bone samples, which both are normalized to the carbon-to-carbon bonding intensity at  $1589\text{ cm}^{-1}$  (highlighted by light yellow in the picture),<sup>45–47</sup> show a significant reduction in the C–H bonding between  $2870$  to  $3010\text{ cm}^{-1}$ <sup>48–49</sup> and also O–H bonding between  $3380$  to  $3530\text{ cm}^{-1}$ <sup>45,46,50</sup> of the carbonized bone sample. Moreover, there is some reduction in intensity of the bonding of the carbonized bone related with phosphate ( $PO_4^{3-}\nu_2$ ) around  $422\text{ cm}^{-1}$ , double peak of phosphate antisymmetric bending frequency ( $PO_4^{3-}\nu_4$ ) around  $566$  and  $636\text{ cm}^{-1}$ , proline around  $835\text{ cm}^{-1}$ , phosphate ( $PO_4^{3-}\nu_1$ ) around  $883\text{ cm}^{-1}$ , phosphate ( $PO_4^{3-}\nu_3$ ) around  $1024\text{ cm}^{-1}$ , amide III (primarily from the in-phase combination of NH in-plane bend and CN stretch) around  $1288\text{ cm}^{-1}$ , pentosidine around  $1495\text{ cm}^{-1}$ , and amide I (primarily from the C=O stretch and C–H bending) around  $1687\text{ cm}^{-1}$ .<sup>48,49,51–53</sup> Results of the Raman spectroscopy are in a good agreement with molecular LIBS. Increase in carbon concentration of the carbonized bone sample (obtained from atomic LIBS data) in combination with results of the Raman and molecular LIBS, which show bonding of carbon to carbon has not broken while that of carbon to other elements have broken, indicates that the carbonization has occurred in the carbonized samples.

Figures 3(a) and 3(b) show LIBS spectra of normal and carbonized bone samples, respectively.

As shown in Figs. 3(a) and 3(b), the ratio of the intensities between the sodium (Na) peak at  $321.2\text{ nm}$  (from  $2s^22p^53p$  to  $2s^22p^53s$ ) and the calcium peak at  $612.2\text{ nm}$  (from  $3p^64s5s$  to  $3p^64s4p$ ) is different in normal and carbonized bone. These two prominent peaks with a high difference in intensity ratio in two groups of samples, which had the lowest Wilks' lambda between the observed peak pairs, can be used for differentiation between carbonized and noncarbonized bone. Figure 4 shows

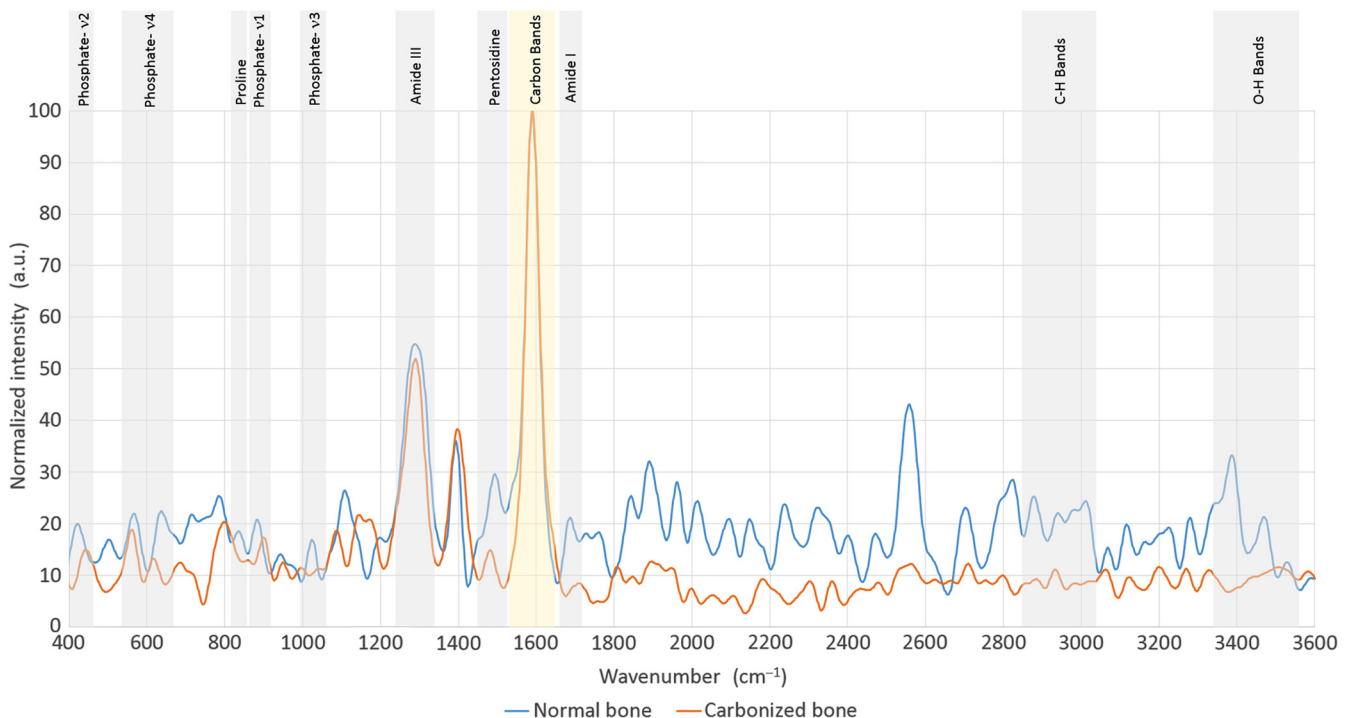
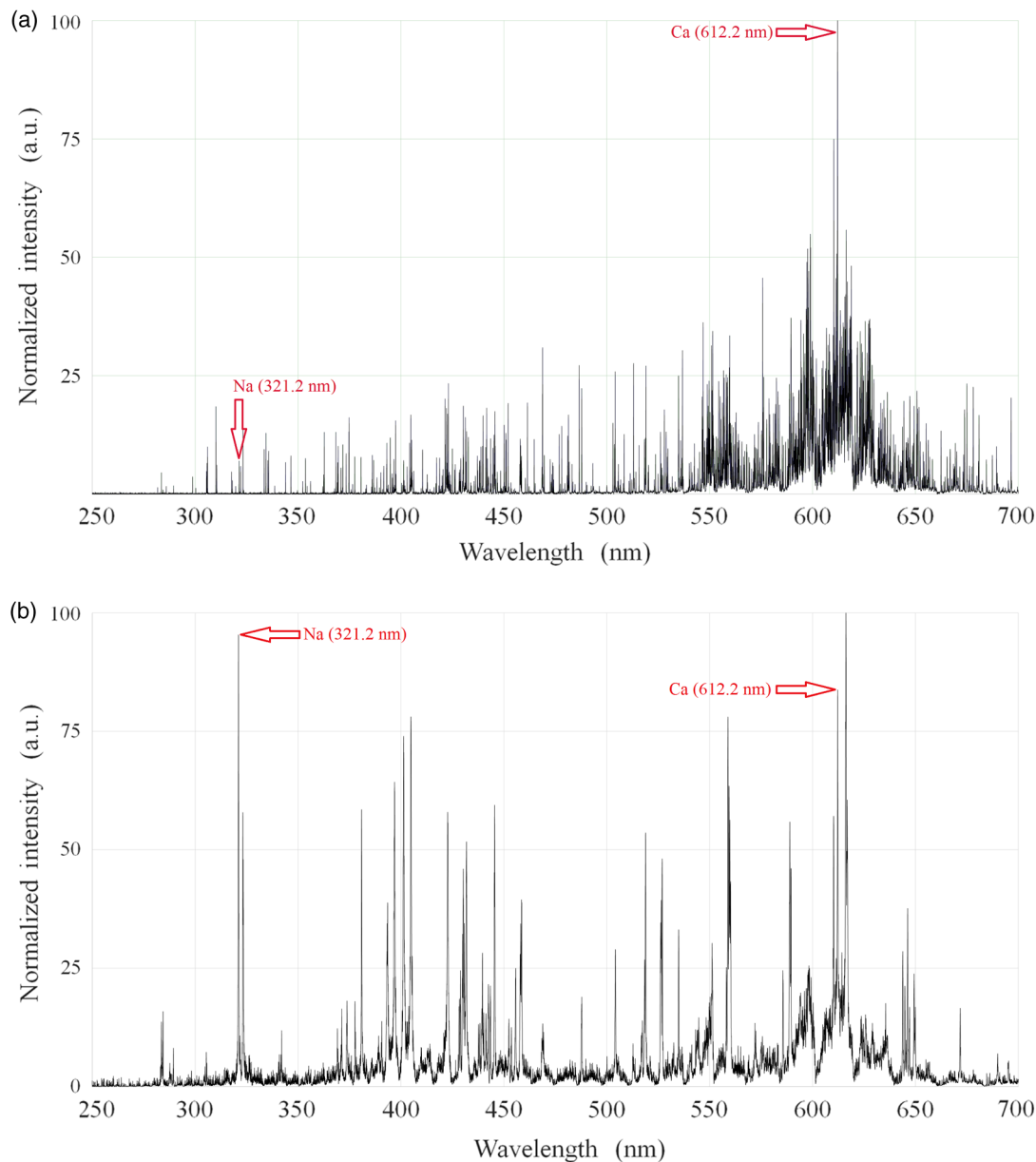


Fig. 2 Raman spectra of normal and carbonized bone samples.



**Fig. 3** LIBS spectra of (a) normal and (b) carbonized bone sample showing selected peak pairs.

the sodium-to-calcium intensity ratio for all samples. The first 50 data points were obtained from sample 1, the second 50 data points from sample 2, and so on, until the last 50 data points from sample 5.

As shown in Fig. 4, most of the ratios related to normal bone are below the threshold line, and most of the ratios related to carbonized bone are above the threshold line. The threshold line was selected in a way to maximize the accuracy of the classifier. Statistical parameters of the classifier, including true positive rate (sensitivity), true negative rate (specificity), positive predictive value (precision), negative predictive value, and accuracy, are shown in Table 1.

As written in the last column of Table 1, all statistical parameters (obtained from 500 spectra) are above 92%. The ROC curve was also plotted, and the area under curve (AUC) was calculated to confirm the performance of the classifier. Figure 5 shows the ROC curve. The AUC of the curve was over 98%.

## 4 Discussion

In this paper, LIBS showed reliable result (accuracy of more than 95%) for carbonization detection in *ex vivo* condition. *Ex vivo* performance of LIBS for detecting carbonized bone seems reliable even with simple ratio-threshold-based methods. Thus, the *ex vivo* results are very likely to transfer also to *in vivo* experiments. However, the achieved accuracy from the *ex vivo* condition is likely to decrease for future *in vivo* experiments, where bone is not so well-prepared. Possible reasons could be the influence of the superficial contamination of the probing surfaces with blood or any rinsing solutions, such as saline or cooling water during the clinical procedures. A possible solution could be employing a double-pulse LIBS system. In double-pulse LIBS, the first pulse can remove the liquid on the focal point; then the second pulse quickly reaches the target surface before the target area is refilled with liquid. From a machine learning point of view, to further increase detection accuracy,

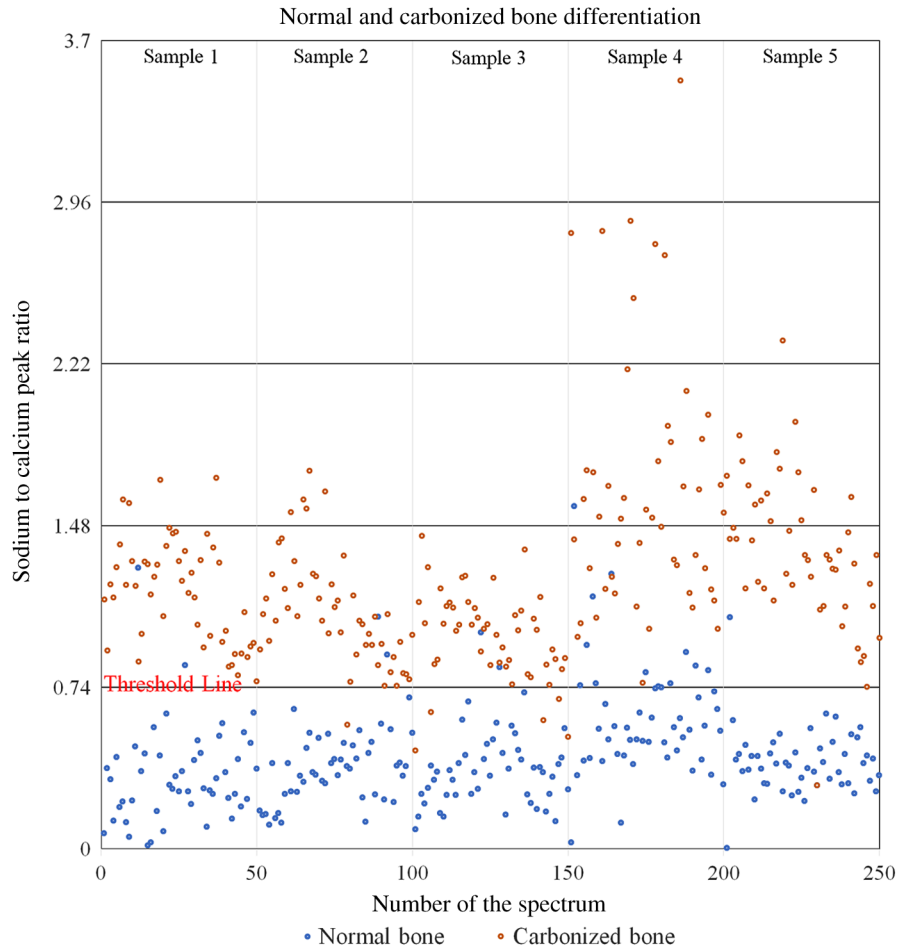


Fig. 4 Sodium-to-calcium intensity ratio for all samples.

Table 1 Statistical parameters of the classifier.

	Sample 1	Sample 2	Sample 3	Sample 4	Sample 5	Total
True positive	50	49	45	50	49	243
False positive	2	2	2	12	1	19
True negative	48	48	48	38	49	231
False negative	0	1	5	0	1	7
True positive rate (sensitivity) (%)	100	98	90	100	98	97
True negative rate (specificity) (%)	96	96	96	76	98	92
Positive predictive value (precision) (%)	96	96	96	81	98	93
Negative predictive value (%)	100	98	91	100	98	97
Accuracy (%)	98	97	93	88	98	95

more complex classifiers could be used that, e.g., also involve additional intensities of other elements. While the number of false positives in this experiment was very low (19 out of 500), but false positives are not a real issue in this case. From a safety point of view, it is better to assume that carbonization has occurred and increases irrigation to avoid future

carbonization at the cost of a reduced cutting speed. In the current experiment, the soft tissue was carefully removed from the surface of the bone using a surgical scalpel, but it is suggested to consider the first initial shots as a cleaning shot. Although it has been reported that the type of nutrition and also age may influence the elemental composition of the tissues, this will not

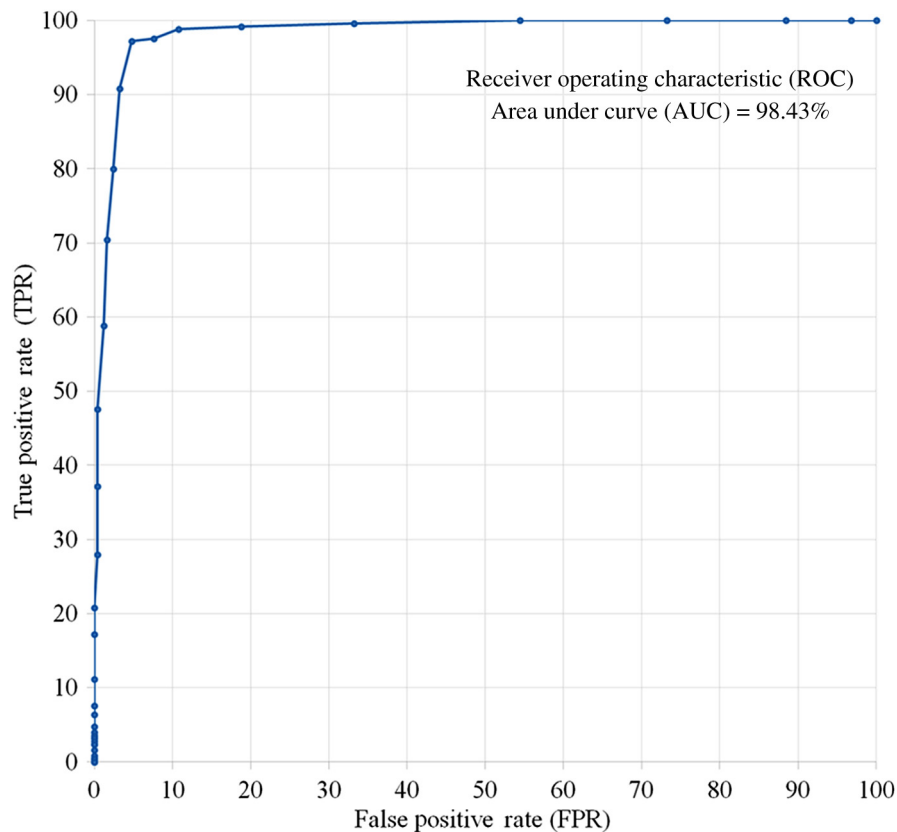


Fig. 5 ROC curve.

significantly influence the differentiation performance in this study because only the most prominent emission lines were considered for classification.<sup>33,39</sup> However, the differentiation performance could be improved by considering the average of multiple spectra for the analysis, but using multiple spectra in a real-time application is time-consuming both for collection and also data analysis. Moreover, it should be considered that using multiple spectra is a trade-off between the damage caused during the collection/calculation time and the increase in differentiation accuracy. Finally, it is worth noting that in this pilot study, a well-carbonized bone was used as a sample; therefore, in the further studies, the performance of the technique should also be evaluated with less carbonized samples to confirm the applicability of the proposed method.

## 5 Conclusion

The preliminary results of this study demonstrate that LIBS is a powerful technique for autocarbonization detection under *ex vivo* conditions by monitoring the plasma plumes occurring during laserosteotomy procedures. Based on the previous reports, the elements detected during the ablation were in agreement with those expected to be found in the elemental composition of bone. The intensity ratio of sodium and calcium enabled successful differentiation of carbonized bone from noncarbonized bone with high accuracy. Sensitivity and specificity of 97% and 92% were achieved, respectively. Therefore, this suggests that carbonization monitoring during laserosteotomy could be successfully achieved using an LIBS-based detection system. However, further research will be needed to confirm the potential *in vivo* clinical applicability of the proposed method.

## Disclosures

The authors have no potential conflicts of interest to declare in this paper.

## Acknowledgments

The authors gratefully acknowledge funding of the Werner Siemens Foundation through the Minimally Invasive Robot-Assisted Computer-Guided Laserosteotomy (MIRACLE) project. Moreover, the authors are particularly appreciative of the assistance given by Ms. Shohreh Khatami.

## References

1. G. R. Gunaratne et al., "A review of the physiological and histological effects of laser osteotomy," *J. Med. Eng. Technol.* **41**(1), 1–12 (2017).
2. K.-W. Baek et al., "A comparative investigation of bone surface after cutting with mechanical tools and Er:YAG laser," *Lasers Surg. Med.* **47**(5), 426–432 (2015).
3. K.-W. Baek et al., "Clinical applicability of robot-guided contact-free laser osteotomy in cranio-maxillo-facial surgery: in-vitro simulation and in-vivo surgery in minipig mandibles," *Br. J. Oral Maxillofac. Surg.* **53**(10), 976–981 (2015).
4. N. Jowett et al., "Bone ablation without thermal or acoustic mechanical injury via a novel picosecond infrared laser (PIRL)," *Otolaryngology* **150**(3), 385–393 (2014).
5. C.-A. Tulea et al., "Highly efficient nonthermal ablation of bone under bulk water with a frequency-doubled Nd:YVO<sub>4</sub> picosecond laser," *Proc. SPIE* **8565**, 85656E (2013).
6. C.-A. Tulea et al., "Laser cutting of bone tissue under bulk water with a pulsed ps-laser at 532 nm," *J. Biomed. Opt.* **20**(10), 105007 (2015).
7. A. Pourzarandian et al., "Histological and TEM examination of early stages of bone healing after Er:YAG laser irradiation," *Photomed. Laser Ther.* **22**(4), 342–350 (2004).

8. L. Beltrán et al., "Effect of laser pulse duration on ablation efficiency of hard bone in microseconds regime," *Proc. SPIE* **10453**, 104531S (2017).
9. J. T. Walsh, T. J. Flotte, and T. F. Deutsch, "Er:YAG laser ablation of tissue: effect of pulse duration and tissue type on thermal damage," *Lasers Surg. Med.* **9**(4), 314–326 (1989).
10. Y.-M. Lee et al., "Average-power mediated ultrafast laser osteotomy using a mode-locked Nd:YVO<sub>4</sub> laser oscillator," *J. Biomed. Opt.* **12**(6), 060505 (2007).
11. D. Kundrat et al., "Endoluminal non-contact soft tissue ablation using fiber-based Er:YAG laser delivery," *Proc. SPIE* **9702**, 97020E (2016).
12. Y. Zhang et al., "Dependence of ablation depth on angle of incidence for hard tissue ablation using pulsed CO<sub>2</sub> laser," in *European Conf. on Biomedical Optics*, Paper No. 809216 (2011).
13. Y. Liu and M. Niemz, "Ablation of femoral bone with femtosecond laser pulses—a feasibility study," *Lasers Med. Sci.* **22**(3), 171–174 (2007).
14. H. Kang, I. Rizoou, and A. Welch, "Hard tissue ablation with a spray-assisted mid-IR laser," *Phys. Med. Biol.* **52**(24), 7243–7259 (2007).
15. H. Abbasi et al., "Effect of cooling water on ablation in Er:YAG laser-osteotome of hard bone," *Proc. SPIE* **10453**, 104531I (2017).
16. S. A. Boppart et al., "High-resolution optical coherence tomography-guided laser ablation of surgical tissue," *J. Surg. Res.* **82**(2), 275–284 (1999).
17. A. V. Shakhov et al., "Optical coherence tomography monitoring for laser surgery of laryngeal carcinoma," *J. Surg. Oncol.* **77**(4), 253–258 (2001).
18. R. Kanawade et al., "Pilot study of laser induced breakdown spectroscopy for tissue differentiation by monitoring the plume created during laser surgery—an approach on a feedback laser control mechanism," *Spectrochim. Acta Part B* **87**, 175–181 (2013).
19. H. K. Nguendon et al., "Characterization of ablated porcine bone and muscle using laser-induced acoustic wave method for tissue differentiation," *Proc. SPIE* **10417**, 104170N (2017).
20. E. Bay, A. Douplik, and D. Razansky, "Optoacoustic monitoring of cutting efficiency and thermal damage during laser ablation," *Lasers Med. Sci.* **29**(3), 1029–1035 (2014).
21. F. Stelzle et al., "In vivo optical tissue differentiation by diffuse reflectance spectroscopy: preliminary results for tissue-specific laser surgery," *Surg. Innov.* **19**(4), 385–393 (2012).
22. F. Stelzle et al., "Diffuse reflectance spectroscopy for optical soft tissue differentiation as remote feedback control for tissue-specific laser surgery," *Lasers Surg. Med.* **42**(4), 319–325 (2010).
23. F.-Y. Yueh et al., "Preliminary evaluation of laser-induced breakdown spectroscopy for tissue classification," *Spectrochim. Acta Part B* **64**(10), 1059–1067 (2009).
24. D. C. Jeong, P. S. Tsai, and D. Kleinfeld, "Prospect for feedback guided surgery with ultra-short pulsed laser light," *Curr. Opin. Neurobiol.* **22**(1), 24–33 (2012).
25. K. Henn et al., "A spectroscopic approach to monitor the cut processing in pulsed laser osteotomy," *Lasers Med. Sci.* **28**(1), 87–92 (2013).
26. L. A. Reisner et al., "A prototype biosensor-integrated image-guided surgery system," *Int. J. Med. Rob. Comput. Assisted Surg.* **3**(1), 82–88 (2007).
27. P. C. Ashok et al., "A Raman spectroscopy bio-sensor for tissue discrimination in surgical robotics," *J. Biophotonics* **7**(1–2), 103–109 (2014).
28. A. Douplik et al., "Limitations of cancer margin delineation by means of autofluorescence imaging under conditions of laser surgery," *J. Innovative Opt. Health Sci.* **3**(1), 45–51 (2010).
29. F. Krause et al., "Evaluation of selective calculus removal by a fluorescence feedback-controlled Er:YAG laser in vitro," *J. Clin. Periodontol.* **34**(1), 66–71 (2007).
30. F. Mehari et al., "Laser induced breakdown spectroscopy for bone and cartilage differentiation-ex vivo study as a prospect for a laser surgery feedback mechanism," *Biomed. Opt. Express* **5**(11), 4013–4023 (2014).
31. F. Mehari et al., "Investigation of laser induced breakdown spectroscopy (LIBS) for the differentiation of nerve and gland tissue—a possible application for a laser surgery feedback control mechanism," *Plasma Sci. Technol.* **18**(6), 654–660 (2016).
32. F. Mehari et al., "Investigation of the differentiation of ex vivo nerve and fat tissues using laser-induced breakdown spectroscopy (LIBS): prospects for tissue-specific laser surgery," *J. Biophotonics* **9**(10), 1021–1032 (2016).
33. M. Rohde et al., "The differentiation of oral soft-and hard tissues using laser induced breakdown spectroscopy—a prospect for tissue specific laser surgery," *J. Biophotonics* **10**, 1250–1261 (2017).
34. F. Scholkmann et al., "A review on continuous wave functional near-infrared spectroscopy and imaging instrumentation and methodology," *NeuroImage* **85**, 6–27 (2014).
35. M. Nazeri et al., "Laser-induced breakdown spectroscopy via the spatially resolved technique using non-gated detector," *J. Russ. Laser Res.* **37**(2), 164–171 (2016).
36. J. E. Sansonetti and W. C. Martin, "Handbook of basic atomic spectroscopic data," *J. Phys. Chem. Ref. Data* **34**(4), 1559–2259 (2005).
37. R. K. Gill et al., "Preliminary fsLIBS study on bone tumors," *Biomed. Opt. Express* **6**(12), 4850–4858 (2015).
38. O. Samek et al., "Quantitative laser-induced breakdown spectroscopy analysis of calcified tissue samples," *Spectrochim. Acta Part B* **56**(6), 865–875 (2001).
39. M. Tofaneli et al., "Spectroscopic analysis of bones for forensic studies," *Spectrochim. Acta Part B* **99**, 70–75 (2014).
40. R. K. Gill et al., "The effects of laser repetition rate on femtosecond laser ablation of dry bone: a thermal and LIBS study," *J. Biophotonics* **9**(1–2), 171–180 (2016).
41. J. H. Han et al., "Differentiation of cutaneous melanoma from surrounding skin using laser-induced breakdown spectroscopy," *Biomed. Opt. Express* **7**(1), 57–66 (2016).
42. H. Huang et al., "Smart surgical tool," *J. Biomed. Opt.* **20**(2), 028001 (2015).
43. M. Kasem et al., "Effect of the wavelength on laser induced breakdown spectrometric analysis of archaeological bone," *Spectrochim. Acta Part B* **101**, 26–31 (2014).
44. D. Santos et al., "Evaluation of femtosecond laser-induced breakdown spectroscopy for analysis of animal tissues," *Appl. Spectrosc.* **62**(10), 1137–1143 (2008).
45. B. D. Mistry, *A Handbook of Spectroscopic Data, Chemistry (UV, IR, PMR, CNMR and Mass Spectroscopy)*, Oxford Book Company, Jaipur (2009).
46. Z. Movasaghi et al., "Raman spectroscopy of biological tissues," *Appl. Spectrosc. Rev.* **42**(5), 493–541 (2007).
47. K. Kochan et al., "Pathological changes in the biochemical profile of the liver in atherosclerosis and diabetes assessed by Raman spectroscopy," *Analyst* **138**(14), 3885–3890 (2013).
48. M. D. Morris et al., "Recent developments in Raman and infrared spectroscopy and imaging of bone tissue," *Spectroscopy* **18**(2), 155–159 (2004).
49. M. D. Morris et al., "Raman assessment of bone quality," *Clin. Orthop. Relat. Res.* **469**(8), 2160–2169 (2011).
50. P. Meksiarun et al., "Comparison of multivariate analysis methods for extracting the paraffin component from the paraffin-embedded cancer tissue spectra for Raman imaging," *Sci. Rep.* **7**, 44890 (2017).
51. E. P. Paschalis et al., "Vibrational spectroscopic techniques to assess bone quality," *Osteoporosis Int.* **28**(8), 2275–2291 (2017).
52. J. W. Ager et al., "Deep-ultraviolet Raman spectroscopy study of the effect of aging on human cortical bone," *J. Biomed. Opt.* **10**(3), 034012 (2005).
53. M. D. Morris et al., "Kerr-gated time-resolved Raman spectroscopy of equine cortical bone tissue," *J. Biomed. Opt.* **10**(1), 014014 (2005).

Biographies for the authors are not available.